International Journal of Control

ISSN: 0020-7179 (Print) 1366-5820 (Online) Journal homepage: https://www.tandfonline.com/loi/tcon20

Controllability and observability of 2D thermal flow in bulk storage facilities using sensitivity fields

Nik L.M. Grubben & Karel J. Keesman

To cite this article: Nik L.M. Grubben & Karel J. Keesman (2018) Controllability and observability of 2D thermal flow in bulk storage facilities using sensitivity fields, International Journal of Control, 91:7, 1554-1566, DOI: 10.1080/00207179.2017.1321782

To link to this article: https://doi.org/10.1080/00207179.2017.1321782

Published online: 11 May 2017.

INTERNATIONAL JOURNAL OF CONTROL
2018, VOL. 91, NO. 7, 1554–1566
https://doi.org/10.1080/00207179.2017.1321782

Taylor & Francis
Taylor & Francis Group

Controllability and observability of 2D thermal flow in bulk storage facilities using sensitivity fields

Nik L.M. Grubben[a,b] and Karel J. Keesman[b]

[a]Omnivent Techniek B.V., Zeewolde, The Netherlands; [b]Biobased Chemistry and Technology, Wageningen University, Wageningen, The Netherlands

ABSTRACT

To control and observe spatially distributed thermal flow systems, the controllable field and observable field around the actuator and sensor are of interest, respectively. For spatially distributed systems, the classical systems theoretical concepts of controllability and observability are, in general, difficult to apply. In this study, sensitivity fields were used to analyse the behaviour from input to state and from initial state to output. For the analysis of controllability and observability, a large-scale, bulk storage facility with coupled thermal flow of air and agro-products was used. Analysis of this system using the classical systems theory results in controllability and observability results that are dependent on the step size of the spatially discretised system. Due to matrix multiplications, inaccurate results are calculated if the step size is too small. Our findings indicate that input-state and initial-state output sensitivity fields provide sufficient information about the controllability and observability of large coupled spatially distributed systems, using finite-dimensional state space representation with small discretisation steps.

ARTICLE HISTORY
Received 16 December 2016
Accepted 17 April 2017

KEYWORDS
Spatially distributed coupled systems; convection–diffusion–reaction equations; sensitivity field; controllability; observability

Nomenclature

$\boldsymbol{A}$	State matrix
a_a	Diffusion coefficient in air
a_p	Diffusion coefficient in product
$\boldsymbol{B}$	Input matrix
$\boldsymbol{C}$	Output matrix
$\boldsymbol{\mathcal{C}}$	Controllability matrix
c	Convection coefficient in air
$\boldsymbol{D}$	Feed-forward matrix
h	Step size
L	Length
$\boldsymbol{M}$	Matrix
n	Coordinates
$\boldsymbol{\mathcal{O}}$	Observability matrix
$\mathcal{P}$	Péclet number
r	Reaction coefficient
$\boldsymbol{S}$	Sensitivity field
T	Temperature
t	Time
$\mathcal{T}$	Final time
$\boldsymbol{u}$	Input vector
v	Velocity
$\boldsymbol{W}_c$	Controllability Gramian
$\boldsymbol{W}_o$	Observability Gramian
$\boldsymbol{X}$, $\boldsymbol{x}$	State vector
$\dot{\boldsymbol{x}}$	Time differentiated state vector
$\boldsymbol{y}$	Output vector
z	Coordinates
α	Input
Δ	Laplace operator
κ	Condition number
λ	Eigenvalue
μ	Weighted singular value
∇	Vector differential operator nabla
τ	Response time
σ	Singular value

1. Introduction

Convection–diffusion–reaction (CDR) equations are used to describe the dynamic behaviour of mass and energy in a wide range of physical systems, such as, for instance, heat exchangers, flow systems, all types of chemical reactors, but also bulk food-storage systems (see e.g. Chourasia & Goswami, 2007; Garzon-Alvarado, Galeano, & Mantilla, 2012; Lopes & Quita-Ferreira, 2011; Nagarajan, Chen, Wang, & Ma, 2015). In these systems, physical phenomena, such as the transfer of momentum, mass, energy or other physical quantities, typically occur within the system and through the system boundaries. To have some influence and information on these systems they are controlled and observed (see e.g. Brecht, Quanten, Zerihundesta, Buggenhout, & Berckmans,

CONTACT Karel J. Keesman karel.keesman@wur.nl

2005; Dochain, Couenne, & Jallut, 2009; Mohammadi, Aksikas, Dubljevic, & Forbes, 2012). For proper control and sensing of such systems, controllability and observability play central roles (Storkaas & Skogestad, 2007; Varga, Hangos, & Szigeti, 1995).

This article focuses on systems theoretical properties of one- and two-dimensional (i.e. 1D and 2D) thermal flow in porous media, as in, for example, bulk food-storage facilities (Grubben & Keesman, 2015). In such systems, flow is often described by the law of conservation of momentum, and continuity equation in one, two or three dimensions (Chourasia & Goswami, 2007). Other transport phenomena, such as mass and energy transfer in the bulk, and between the food bulk and the air, are described by the laws of conservation for mass and energy, and constitutive laws. The modelling of such dynamic- and spatially distributed systems most often results in a set of coupled, non-linear, partial differential equations (PDEs) that must be solved numerically.

In our specific example of a bulk food-storage facility used for the storage of potatoes, onion or wheat, the practical goal is to maintain the quality of the food products at a certain level for a longer time. Due to the interaction between the climate in the facility and the food product itself, the product quality is controlled by the climate, whereas the climate inside of the bulk is controlled by forced- or natural convection of air. In practice, and in the case of forced convection, most often, air with a piecewise constant flow rate is supplied. The air is streamed from the bottom of the bulk, through the porous medium (bulk matter), to the top layer of the bulk. From there, it either leaves the facility through an outlet or is recirculated (Figure 1).

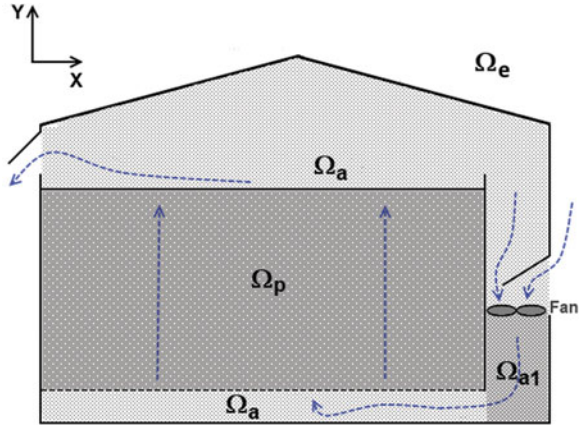

Figure 1. 2D configuration of a bulk storage facility. The climate is controlled by ventilating air from bottom to top through the porous medium. Here, Ω_a is the air domain, Ω_{a1} the pressure chamber, Ω_p the porous medium domain and Ω_e the environment.

In the following, only thermal flow due to forced convection with zero or constant air velocity is considered. Hence, from a theoretical system perspective, a piece-wise, linear time-invariant (LTI), 2D coupled CDR system is obtained. The system states taken into consideration are the temperature of the air (T_a) and the temperature of the product (T_p), more precisely $T_a(z, t)$ and $T_p(z, t)$, where z represents the spatial coordinate and t time. From practice, it is known that these systems are unstable, due to biological processes. For instance, rotting- and ageing processes of the product are non-reversible, although these processes can be stabilised by recirculating air. State-of-the-art control in storage facilities aims to maintain temperature, and sometimes humidity, around a certain pre-specified level to prevent rotting and to diminish moisture loss and the effects of ageing. Novel control concepts, however, aim to control product quality directly (Grubben & Keesman, 2015). In addition, it is preferable to have a homogeneous quality in the entire bulk, whilst minimising ventilation costs. These requirements necessitate a model-based control strategy. However, before designing such a control strategy, the key question is: Can the internal states of the system, T_a and T_p, move from any initial-state to any other final-state in finite time? If this is the case, the system is referred to as *controllable*.

Formally, from a systems theory perspective, the system is said to be controllable if, and only if, it is possible to transfer the system from the zero state $x(t_0)$, at any initial time t_0, to any terminal state $x(t_1) = x_1$ within a finite time $t_1 - t_0$ (Kwakernaak & Sivan, 1972). For the bulk storage system, this implies that at a specific time instant, it would be possible to create an arbitrary temperature profile, in, for instance, the vertical direction. In bulk-food storage practices, however, such a requirement is too strict. Therefore, the formal definition of controllability is not appropriate in this case.

To obtain current information about the states in the system, some observations should be available. In systems theory, a system is referred to as observable, if, and only if, it is possible to determine any (arbitrary) initial state $x(t_0) = x_0$ by using only finite output data records $y(t)$ for $t_0 \leq t \leq t_1$ (Friedland, 2005). For sensor location in a spatially distributed system, however, the systems theoretical concept of observability does not provide sufficient information. In practice, for spatially distributed systems, the observable field around the sensor would be of interest. In conclusion, for practical insight into spatially distributed systems, the systems theoretical concepts of controllability and observability provide insufficient insight.

For relatively simple, linear CDR systems, infinite-dimensional system theory (Curtain & Zwart, 1995) could be used to analyse the controllability and

observability in depth (see Jai, Simon, Zerrik, & Pritchard, 1995 and Amouroux, Jai, & Zerrik, 1994, respectively). For coupled CDR systems, as in this case, with complex coupled dynamics between air and product in the storage facility, this theory is commonly not applicable.

The objective of this paper is to provide more information about the spatial distribution of air- and product temperature in bulk storage facilities, for actuation and sensing. The concepts of controllability and observability are investigated by analysing the behaviour from input to state and from initial-state to output of a dynamic, spatially distributed system. The input-to-state analysis gives the relation between the control input, generated by the actuator, to the state variables over time, and over the entire spatial domain. The initial-state-to-output analysis provides the relation between the sensor output and the initial-state over time, and over the entire spatial domain. In the paper, these relationships are investigated using sensitivity analysis (SA), see e.g. Tomovic (1963) or Saltelli, Chan, and Scott (2000).

A local SA of our CDR system, using partial derivatives of the state-to-input or output-to-initial-state, led to the study of in- and output sensitivity fields. By spatially discretising the set of partial differential equations, describing heat transfer in the bulk storage, a large set of ordinary differential equations is obtained. In such a case, typically a direct method (DM) SA (Dickinson & Gelinas, 1976) can be carried out.

The outline of the paper is as follows. First, in Section 2, some background on the systems theoretical concepts of controllability and observability for CDR systems, using a state-space representation, is presented. A singular value decomposition (SVD) of the resulting controllability and observability matrices provides some further insights compared to the conventional controllability and observability analyses. However, the SVD-based controllability and observability measures are numerical measures, influenced by the discretisation step size. These concepts are illustrated by an analysis of controllability and observability, and singular values corresponding to a 1D CDR system in Section 3. The main contribution of the paper, however, is the construction of in- and output sensitivity fields for CDR systems. First, in Section 4, a single-state, 1D, CDR system is used to illustrate the theory of in- and output sensitivity fields for CDR systems, followed by a detailed analysis of a 2D, coupled, CDR system in Section 5.

2. Systems theory

Classical systems theory can be applied to a wide range of systems. However, for some applications, concepts in systems theory are too strict, and additional information is required. For instance, applying controllability and observability theory on CDR models of temperature in a bulk storage facility only gives a very initial impression of the systems behaviour. In this section, conventional controllability and observability theory, including the SVD of the resulting controllability and observability matrices, will be applied first on a 1D boundary controlled CDR-system to demonstrate the limitations of this theory in practice.

2.1 Controllability and observability for boundary controlled CDR systems

Typically, a boundary controlled CDR system is characterised by the partial differential equation:

$$\left(\frac{\partial \boldsymbol{X}}{\partial t} + \boldsymbol{v}\cdot\nabla\boldsymbol{X}\right) = a\Delta\boldsymbol{X} + \boldsymbol{r}_X \text{ in } (0,t]\times\Omega_d \quad (1)$$

$$\boldsymbol{X} = \boldsymbol{u}_{\text{dirichlet}} \text{ on } (0,t]\times\partial\Omega_{d1} \quad (2)$$

$$\frac{\partial \boldsymbol{X}}{\partial n} = \boldsymbol{u}_{\text{neumann}} \text{ on } (0,t]\times\partial\Omega_{d2} \quad (3)$$

Thus, including Dirichlet (2) and Neumann (3) boundary conditions, at the corresponding boundaries $\partial\Omega_{d1}$ and $\partial\Omega_{d2}$, respectively. Here, $\boldsymbol{X}\in\mathbb{R}^N$ is a state vector, t represents time, $\boldsymbol{v}$ is the velocity vector, c the diffusion coefficient, $\boldsymbol{r}_X$ a first-order reaction vector, $\boldsymbol{u}_{\text{dirichlet}}$ is the input $\boldsymbol{u}$ on boundary $\partial\Omega_{d1}$ and $\boldsymbol{u}_{\text{neumann}}$ the flux through the boundary $\partial\Omega_{d2}$. For the three-dimensional (3D) case; $\nabla = [\frac{\partial}{\partial x}\ \frac{\partial}{\partial y}\ \frac{\partial}{\partial z}]^T$ and $\Delta := \nabla^2 = [\frac{\partial^2}{\partial x^2} + \frac{\partial^2}{\partial y^2} + \frac{\partial^2}{\partial z^2}]$. Discretisation in space results in a state vector $X\in\mathbb{R}^n$ containing the set of state variables X for every grid point $i = 1,\ldots,I$. In our example, $\boldsymbol{v}$ is constant and, thus, the Equation (1) is approximated by a set of $n = NI$ first-order linear differential equations: extending the set of differential equations with a set of algebraic output equations gives:

$$\begin{aligned}\dot{\boldsymbol{x}}(t) &= \boldsymbol{A}\boldsymbol{x}(t) + \boldsymbol{B}\boldsymbol{u}(t)\\ \boldsymbol{y}(t) &= \boldsymbol{C}\boldsymbol{x}(t) + \boldsymbol{D}\boldsymbol{u}(t)\end{aligned} \quad (4)$$

Here, $\boldsymbol{x} = [x_1, x_2, \ldots, x_n]^T \in \mathbb{R}^n$ is the spatially discretised state vector of the system with $x(0) = x_0$, $\boldsymbol{u} = [u_1, u_2, \ldots, u_m]^T \in \mathbb{R}^m$ is the input vector and $\boldsymbol{y} = [y_1, y_2, \ldots, y_p]^T \in \mathbb{R}^p$ is the output vector. Furthermore, the matrices $\boldsymbol{A}, \boldsymbol{B}, \boldsymbol{C}$ and $\boldsymbol{D}$ in the LTI system (4) are of appropriate dimensions. As follows, the $n\times n$ system matrix $\boldsymbol{A}$ requires special attention. If, however, $\boldsymbol{v}$ is not constant, a linearisation step is needed, most often leading to a LTV (linear time-varying) system.

The LTI system (4) is controllable, if, and only if, the rank of the controllability matrix:

$$\boldsymbol{\mathcal{C}} = [\boldsymbol{B}\ \boldsymbol{AB}\ \boldsymbol{A}^2\boldsymbol{B}\ \cdots\ \boldsymbol{A}^{n-1}\boldsymbol{B}] \tag{5}$$

is equal to n, so of full (row) rank (Kalman, 1959). The controllability matrix multiplied with its transpose gives the $n \times n$ controllability Gramian:

$$\boldsymbol{W}_c = \boldsymbol{\mathcal{C}}\boldsymbol{\mathcal{C}}^T \tag{6}$$

Similarly, an LTI system is observable, if, and only if, the rank of the observability matrix:

$$\boldsymbol{\mathcal{O}} = \begin{bmatrix} \boldsymbol{C} \\ \boldsymbol{CA} \\ \boldsymbol{CA}^2 \\ \vdots \\ \boldsymbol{CA}^{n-1} \end{bmatrix} \tag{7}$$

is equal to n, so in this case of full (column) rank (Kalman, 1959). The transpose of the observability matrix post multiplied with $\boldsymbol{\mathcal{O}}$ gives the $n \times n$ observability Gramian:

$$\boldsymbol{W}_o = \boldsymbol{\mathcal{O}}^T\boldsymbol{\mathcal{O}} \tag{8}$$

Consequently, given (1) with constant velocity vector $\boldsymbol{v}$, state discretisation rank tests provide strict controllability and observability information on the LTI system.

2.2 Singular value decomposition

Controllability and observability theory, as presented in the previous section, gives satisfying information about the relation between the inputs and states, and outputs and states, but only in terms of true or false. As demonstrated in the following, a numerical rank test on the controllability and observability matrices will give further insight. As such, a SVD of the Gramian of $\boldsymbol{\mathcal{C}}$ and $\boldsymbol{\mathcal{O}}$ may give this additional information.

In general, the singular values of a rectangular matrix provide a near-singularity measure. For instance, for a non-square matrix $\boldsymbol{M}$ the decomposition provides insight in the contribution of each element in each direction, determined by the left- and right singular vectors. The SVD of an $\widetilde{m} \times \widetilde{n}$ matrix $\boldsymbol{M}$ is defined as:

$$\boldsymbol{M} = \boldsymbol{U}\boldsymbol{\Sigma}\boldsymbol{V}^T \tag{9}$$

Here, $\boldsymbol{U}$ is a $\widetilde{m} \times \widetilde{m}$ orthogonal matrix (containing left singular vectors), $\boldsymbol{V}$ is a $\widetilde{n} \times \widetilde{n}$ orthogonal matrix with right singular vectors and $\boldsymbol{\Sigma}$ is a $\widetilde{m} \times \widetilde{n}$ pseudo-diagonal matrix with the singular values σ_i on the diagonal, which are sorted as $\sigma_1 \geq \sigma_2 \geq \cdots \geq \sigma_{\min(\widetilde{m},\widetilde{n})}$. The singular values are the square-roots of the eigenvalues of $\boldsymbol{MM}^{\boldsymbol{T}}$:

$$\sigma_i = \sqrt{\lambda_i(\boldsymbol{MM}^{\boldsymbol{T}})}, \quad i = 1, \ldots, \min(\widetilde{m}, \widetilde{n}) \tag{10}$$

The SVD of $\boldsymbol{\mathcal{C}}$ and $\boldsymbol{\mathcal{O}}$, respectively, can be used to quantify the controllable- and observable states. For example, uncontrollable states, possibly after applying a state transformation (Doren, Hof, Bosgra, & Jansen, 2013), can be found from the null space of $\boldsymbol{\mathcal{C}}$, which is spanned by the i-th columns of $\boldsymbol{V}$ corresponding to the zero singular values σ_i. Similarly, unobservable states can be found from the null space of $\boldsymbol{\mathcal{O}}$. Extending the tests to near-zero singular values allows the detection of states that are very difficult to control or estimate from observed input-output data.

2.3 A 1D CDR system

For further insight into the controllability and observability properties of a physical system for the heat transfer, an air temperature balance of a porous medium with convection, diffusion and reaction terms is used. In the first analysis, the system is 1D and has a Dirichlet boundary condition for $z = 0$ and a Neumann boundary conditions for $z = L$. Hence, the complete system is defined by:

$$\begin{aligned} \frac{\partial T}{\partial t} &= a\frac{\partial^2 T}{\partial z^2} - c\frac{\partial T}{\partial z} - rT \\ T(t,0) = \alpha, \quad \frac{\partial T}{\partial z}(t,L) &= 0 \end{aligned} \tag{11}$$

Here, T is the air temperature. For a specific, potato bulk storage facility (see Grubben & Keesman, 2015, Lukasse, de Kramer-Cuppen, & Voort, 2007): $a = 0.00002$ (m^2/s), $c = 1$ (m/s), $r = 1$ (1/s), $\alpha = 1$ (K) and $L = 1$ (m). For relatively simple partial differential equations, such as (11), linear infinite- dimensional system theory (Curtain & Zwart, 1995) could be used. However, for complex, coupled systems, analytical solutions become intractable. Therefore, (11) and in the following equations, such as: (11), are discretised in space using central difference methods, leading to:

$$\begin{aligned} \dot{T}(t,z_i) = a\frac{T(t,z_{i-1}) - 2T(t,z_i) + T(t,z_{i+1})}{\Delta h^2} \\ -c\frac{-T(t,z_{i-1}) + T(t,z_{i+1})}{2\Delta h} - rT(t,z_i) \end{aligned} \tag{12}$$

Here, $z_i = i\Delta h$ is the distance from $z = 0$, $i = 0, 1, 2, \ldots, I - 1$ with I total amount of grid points and $\Delta h = \frac{L}{I-1}$

the step size with L total length. A central differential method gives a more accurate solution compared to the forward- or backward difference method, due to the second-order accuracy on h (truncation error). Notice that $a \ll c$, which results in a large Péclet number $Pe = \frac{cL}{a}$ and consequently, a large mesh Péclet number $\mathcal{P} = \frac{c\Delta h}{a}$. This large Péclet number results in a non-monotonous discretised state matrix $\boldsymbol{A}$. In numerical calculations, this may easily lead to oscillatory behaviour, shown as follows. Rearranging the right-hand side of (12):

$$\frac{a}{\Delta h^2}\left[\left(\frac{\mathcal{P}}{2}+1\right)(T(t,z_{i-1})-T(t,z_i))+\left(-\frac{\mathcal{P}}{2}+1\right)\times(T(t,z_{i+1})-T(t,z_i))-\frac{\Delta h^2}{a}rT(t,z_i)\right] \tag{13}$$

A monotonous, tri-diagonal $\boldsymbol{A}$ matrix is obtained if $|\mathcal{P}| < 2$. To satisfy this condition for system (11), with high convection and low diffusion rates, a very small step size Δh, ($I = 25,000$) should be used. If this small step size is used, numerical calculations of the system theory result in numerical errors. Therefore, a step size should be selected that is appropriate for the matrix calculations and results in minimal oscillatory solution. Another, but less accurate, method to avoid oscillations is to use a central-upstream differential scheme (Lynch, 2005). However, this method is not appropriate for our case, due to the repetitive multiplications of the $\boldsymbol{A}$ matrix in (5) and (7) for the controllability and observability tests.

3. Controllability and observability of a 1D CDR system

The system theory discussed in Section 2 is now applied to a 1D CDR system. The 1D system basically represents the porous medium domain, as de-pictured in Figure 1, with constant vertical flow.

3.1 Controllability and observability

Controllability and observability theory leads to a separation of the state space $\mathbb{R}^n$ into two spaces: the controllable/observable and the non-controllable/non-observable subspace. Commonly, these subspaces are determined numerically and, thus, the result depends on the numerical tolerance. For decreasing grid size steps, the values in the tri-diagonal system matrix $\boldsymbol{A}$ increase, which causes an increase in the dimension of the non-controllable space. For instance, in Matlab R2015b, the tolerance of the rank determination is calculated as: tolerance $= \max(size(\boldsymbol{\mathcal{C}}) * eps(\text{norm}(\boldsymbol{\mathcal{C}}))$, where *norm* is the 2-norm of matrix $\boldsymbol{\mathcal{C}}$ ($||\boldsymbol{\mathcal{C}}||_2$), and *eps* specifies the distance from 1.0 to the next largest double-precision number, that is $eps = 2^{(-52)} \approx 2.22e^{(-16)}$. For the 1D CDR system (11) with single-input and single-output (SISO):

$$\boldsymbol{A} = \begin{bmatrix} -\frac{2a}{h^2}+r & -\frac{c}{2h}+\frac{a}{h^2} & 0\cdots & 0 \\ \frac{c}{2h}+\frac{a}{h^2} & -\frac{2a}{h^2}+r & -\frac{c}{2h}+\frac{a}{h^2} & \vdots \\ 0 & \ddots & \ddots & \ddots & 0 \\ \vdots & \frac{u}{2h}+\frac{a}{h^2} & -\frac{2a}{h^2}+r & -\frac{c}{2h}+\frac{a}{h^2} \\ 0 & \cdots 0 & \frac{2a}{h^2} & -\frac{2a}{h^2}+r \end{bmatrix}$$

$$\boldsymbol{B} = \begin{bmatrix} \alpha\left(\frac{c}{2h}+\frac{a}{h^2}\right) \\ 0 \\ \vdots \\ 0 \end{bmatrix}, \boldsymbol{C} = \begin{bmatrix} 0 & \cdots & 1 & 0 & 0 \end{bmatrix} \tag{14}$$

where $h = \Delta h$. For $a = 0.00002$ (m^2/s), $c = 1$ (m/s), $r = 1$ (1/s), $\alpha = 1$ (K) and $L = 1$ (m), the controllability and observability rank test gives full rank up to a discretisation step size of $L/12$ and $L/13$, respectively:

$$\text{rank}(\boldsymbol{C}) = [\boldsymbol{B}\ \boldsymbol{AB}\ \boldsymbol{A}^2\boldsymbol{B}\ \cdots\ \boldsymbol{A}^{11}\boldsymbol{B}] = 12$$
$$\text{rank}(\boldsymbol{O}) = \begin{bmatrix} \boldsymbol{C} \\ \boldsymbol{CA} \\ \boldsymbol{CA}^2 \\ \vdots \\ \boldsymbol{CA}^{12} \end{bmatrix} = 13 \tag{15}$$

For a smaller step size of, for instance, $L/16$ rank($\boldsymbol{C}$) $= 11$ and rank($\boldsymbol{O}$) $= 10$.

3.2 Singular value decomposition of W_c and W_o

A more detailed analysis can be performed by a SVD of the Gramians of the controllability and observability matrices. Zandvliet et al. (2008), for example, used a SVD of the Gramians in the analysis of a single-phase porous medium flow (LTI) system. Space discretisation of the 1D CDR system, as in Section 2.3, results in a tridiagonal matrix with non-dominant diagonal and potentially oscillating behaviour, if the step size chosen is too large.With too small step size, the numerical SVDs become unstable. The condition number of $\boldsymbol{W_c}$ and $\boldsymbol{W_o}$, respectively, will give an indication which spatial discretisation step size would be appropriate.

The condition number of the rectangular matrix $\boldsymbol{M}$ is defined as the ratio of the maximum ($\sigma_{\max}$) and minimum ($\sigma_{\min}$) singular value, that is

$$\kappa(\boldsymbol{M}) = \frac{\sigma_{\max}(\boldsymbol{M})}{\sigma_{\min}(\boldsymbol{M})} \tag{16}$$

A large condition number implies that matrix $\boldsymbol{M}$ is poorly conditioned, and, thus, a small condition number implies a well-conditioned matrix $\boldsymbol{M}$. From numerical analysis, it is known that if the condition number $\kappa = 10^k$, then up to k digits of accuracy can be lost (Cheney & Kincaid, 2008). It is possible that a large condition number causes the matrix $\boldsymbol{M}$ to become non-invertible due to errors in rounding-off. Hence, if large condition numbers are obtained, small changes in the system parameter can result in a non-invertible matrix. For a convection diffusion system, as in (11) with $a = 0.00002$ $[m^2/s]$, $c = 1$ $[m/s]$ and $r = 1$ $[1/s]$, and step size of 1/12, the condition numbers are:

$$\begin{aligned}\kappa(\boldsymbol{W_c}) &= \frac{\sigma_{\max}(\boldsymbol{W_c})}{\sigma_{\min}(\boldsymbol{W_c})} = 2.7 \cdot 10^{25} \\ \kappa(\boldsymbol{W_o}) &= \frac{\sigma_{\max}(\boldsymbol{W_o})}{\sigma_{\min}(\boldsymbol{W_o})} = 3.8 \cdot 10^{18}\end{aligned} \tag{17}$$

The condition numbers of the controllability and observability matrix are very high, and, therefore, the matrices are poorly conditioned. This poor condition is due to the large Péclet number, which results in wiggles in the discretised system. If the condition number approaches the inverse of the floating point number of the machine 4.5*e*15 (inverse *eps* value), precision cannot be guaranteed (Moler, 2004). Hence, from the perspective of condition number, a larger step size should be chosen, at the expense of a larger discretisation error. Another option to obtain a better conditioned system is to use a forward-central discretzation method. A forward-central method for systems with large Péclet number, in general, results in a system with less wiggles. For further analysis of controllability and observability properties, we will focus on a singular value composition of $\boldsymbol{W_c}$ and $\boldsymbol{W_o}$, respectively. In this case: $\boldsymbol{U} = \boldsymbol{V}$, an $n \times n$ matrix.

The singular values (σ_i) on the diagonal of the matrix $\boldsymbol{\Sigma}$ (9) correspond to the i-th column of the left singular vector U_i. Consequently, every non-zero singular value corresponds to a set of weighting factors in the controllable or observable spatially discretised state space. The weighting factors define directions in the state space. Hence, if, for instance, $\sigma_i = 0$, the corresponding weighting factors in the i-th column of $\boldsymbol{U}$ (9) determine the direction in state space, which is uncontrollable or unobservable. Multiplying the singular value σ_i with the corresponding direction vector $\boldsymbol{U}_i$ gives the contribution in the controllable or observable space, of every grid point:

$$\boldsymbol{\mu}_i = \sigma_i \boldsymbol{U}_i \tag{18}$$

Following van Doren et al. (2013), the sum of the singular value multiplied by the corresponding direction gives the contribution of every grid point:

$$\boldsymbol{\mu} = \sum_{i=1}^{n} \sigma_i \boldsymbol{U}_i \tag{19}$$

Applying this on the controllability (6) and observability (8) Gramians of the CDR system (11), with $L = 1$ and $h = 1/12$ results in $\boldsymbol{\mu}_c$ and $\boldsymbol{\mu}_o$ respectively. From the controllability SVD of the controllability Grammian, it follows that the contribution ($\boldsymbol{\mu_c}$) of the first eight states are the largest and of the same order. Therefore, the first states are influenced most by the input α. The observability SVD for a sensor on $z = 0.9$ (m) show that the contribution ($\boldsymbol{\mu_o}$) of the states six to ten are the largest and of the same order. Therefore, these five states are best observable. In both cases, the states that contribute most show some wiggling behaviour. Hence, we have an initial impression of which states are controllable and observable. However, the analysis does not provide a full quantitative information of the spatial distribution of the input on the states or the output measurement on the state observability.

4. Input and output sensitivities of 1D CDR systems

For spatially distributed CDR systems, classical controllability and observability analysis, even extended with an SVD, as in the previous section, may provide insufficient theoretical information of the system with boundary control. The combination of diffusion, convection and reaction terms of the physical system (11) with large Péclet number causes the discretised system matrix $\boldsymbol{A}$ (14) to have a non-monotonous tridiagonal form. As already mentioned in Section 3.2, a non-monotonous matrix potentially shows oscillating behaviour.

Furthermore, a system is said to be controllable, if it is possible to transfer the system from any state to any other state in finite time. And a system is said to be observable, if it is possible to determine any (arbitrary) initial state by using only finite output data records. However, the theory does not give insight about the time afterwards, or a quantity of the spatial distribution where the system is controllable and observable. Input and output sensitivity fields provide such information. Using a input sensitivity field, the impact of the actuator on every state can be visualised, or at least interpreted. The output sensitivity field can give information about the domain that is observable, given a specific sensor location.

For the LTI state space representation, as defined in (4), the input and output sensitivity fields will be analysed

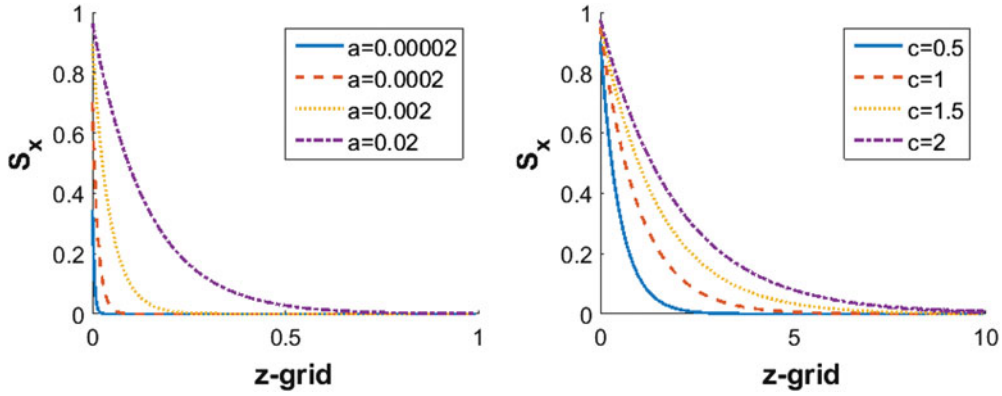

Figure 2. Left, 1D input sensitivity field simulated for different diffusion coefficients without convection, thus $c = 0$. Right: 1D input sensitivity field simulated for different convection coefficients, including diffusion ($a = 0.00002$).

in more detail for $m = p = 1$, thus, the SISO case. All the dynamic relations in the system are covered by (4), and by taking derivatives of the state equation to input and the output to the initial state sensitivities can be calculated in each grid point. Therefore, the DM (Dickinson & Gelinas, 1976) are used to calculate the sensitivities, defined by

$$\boldsymbol{S}_x \triangleq \left(\frac{\partial \boldsymbol{x}}{\partial u}\right), \quad \boldsymbol{S}_y \triangleq \left(\frac{\partial \boldsymbol{y}}{\partial x_o}\right) \tag{20}$$

4.1 Input sensitivity of 1D thermal flow in a bulk storage facility

A direct relation between the sensitivity of the state vector ($\boldsymbol{x}$) with respect to a constant input (u), and denoted as $\boldsymbol{S}_x$, can be derived from the state equation in (4) and is given by:

$$\frac{\partial}{\partial u}\left(\frac{d\boldsymbol{x}}{dt}\right) = \frac{\partial}{\partial u}\left(\boldsymbol{A}\boldsymbol{x} + \boldsymbol{B}u\right), \quad u := \text{constant} \tag{21}$$

$$\frac{d}{dt}\left(\frac{\partial \boldsymbol{x}}{\partial u}\right) = \boldsymbol{A}\frac{\partial \boldsymbol{x}}{\partial u} + \boldsymbol{B} \tag{22}$$

$$\dot{\boldsymbol{S}}_x = \boldsymbol{A}\boldsymbol{S}_x + \boldsymbol{B}, \quad \boldsymbol{S}_x(0) = 0 \tag{23}$$

Consequently, $\boldsymbol{S}_x(t) = \int_0^t e^{\boldsymbol{A}(t-s)}\boldsymbol{B}ds$. Since $\boldsymbol{A}$ is the given system matrix and $\boldsymbol{B}$ depends on the actuator location, the influence of the actuator on every place in the grid on the states in the grid can be determined.

Starting from Equation (11), two different cases can be distinguished. First, we consider the case, in which diffusion dominates, followed by the case, in which convection dominates. For the first case, in which diffusion dominates, four different diffusion rates $a = 0.00002$, $a = 0.0002$, $a = 0.002$, $a = 0.02$ (m^2/s) were selected and, $c = 0$ (m/s), $r = 1$ (1/s) and $\alpha = 1$ [°C]. For the second case, in which convection dominates, $a = 0.00002$ (m^2/s), $r = 1$ (1/s) and $\alpha = 1$ [°C], and four different convection rates $c = 0.5$, $c = 1.0$, $c = 1.5$, $c = 2.0$ (m/s) were selected. The system has a Dirichlet boundary condition at $z = 0$ and a Neumann boundary condition at the end ($z = L$) of the profile. In Figure 2 for dominating diffusion (left) and for dominating convection (right) the steady state values of the sensitivity fields with a discretisation step of $L/200$ are shown.

For the steady state simulations, as shown in Figure 2, a simulation time of ten seconds is used. From the physical knowledge of the system to reach steady state, this simulation time is long enough, due to the large convection rate (1 (m/s)). Figure 3 shows the change of input sensitivity over time in the first seconds. From Figure 3, it can be seen that the sensitivity at $z = 0$ is more or less the same for every simulation time. At time $t = 5$ (s), a steady state is obtained (using $a = 0.00002$ (m^2/s), $c = 1.0$ (m/s), $r = 1$ (1/s), $\alpha = 1$ [°C]), and sensitivity does not increases further. Hence, in this case, with u piece-wise constant on a time interval of 10 (s), the input sensitivity can be directly seen in the right panel of Figure 2. Notice that the steady state sensitivity of the actuator on

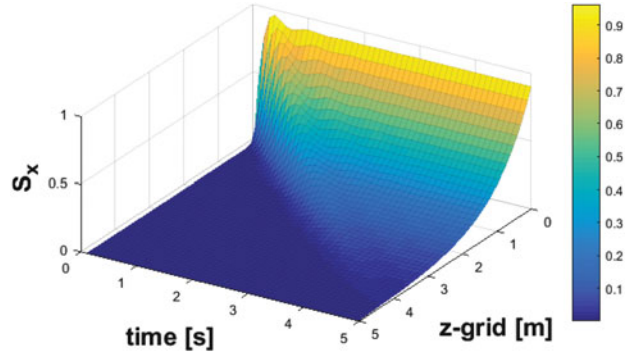

Figure 3. 1D input sensitivity field simulated for 0.1 to 5 seconds, using $a = 0.00002$ (m^2/s), $c = 1.0$ (m/s), $r = 1$ (1/s), $\alpha = 1$ (°C), $L = 5$ (m) and grid size of $\Delta z = L/50$.

the states can be checked from (23):

$$\bar{\boldsymbol{S}}_x = -\boldsymbol{A}^{-1}\boldsymbol{B} \tag{24}$$

The SA of a system with only diffusion-reaction processes provides insight between the diffusion rate and the controllability of the states. For smaller diffusion rates, the effect of the input on the states fades out fast. So, there is some influence from the input to the state only at small distances from the actuator, see left panel of Figure 2. Varying the convection rate in a CDR equation results in comparable results, as a small convection rate results in smaller sensitivities from the input to the state, see right panel of Figure 2. From the results in Figure 2 (left panel), we conclude that a tenfold increase of the diffusion rate will lead to the same sensitivity at roughly three times of the original distance. Doubling the convection rate results in the same sensitivity at roughly two times of the original distance (Figure 2, right panel).

As seen in the left and right panels of Figure 2, the simulations were not conducted for the same length. In the diffusion-reaction case $L = 1$ (m), whilst in the CDR, a length of $L = 10$ (m) was chosen. However, the results show that the length used in different simulations does not affect the magnitude of the steady state values of the sensitivity field.

4.2 Output sensitivity of 1D thermal flow in bulk storage facility

The output of (4) with $\boldsymbol{D} = 0$ is given by:

$$\boldsymbol{y}(t) = \boldsymbol{C}\boldsymbol{x}(t) \tag{25}$$

The solution of an LTI system (4) with $m = p = 1$ (SISO), $u(t) = 0$ for $t < 0$, and $D = 0$ is given by:

$$y(t) = \boldsymbol{C}\left[e^{\boldsymbol{A}t}\boldsymbol{x}(0) + \int_0^t e^{\boldsymbol{A}(t-s)}\boldsymbol{B}u(s)ds\right] \tag{26}$$

The relationship between the output y and the initial-state $\boldsymbol{x}(0)$ can be derived directly from Equation (26). Taking the derivative of the output with respect to the initial-state ($\boldsymbol{x}(0) = \boldsymbol{x}_0$), according to (20),

$$\boldsymbol{S}_y = \frac{dy(t)}{d\boldsymbol{x}_0} = \boldsymbol{C}e^{\boldsymbol{A}t} \tag{27}$$

Hence, for asymptotic stable systems the sensitivity from the output to the initial- state ranges from zero for time to infinity. In the following, instead of $\boldsymbol{S}_y$, the Fisher Infinite Matrix (FIM) is introduced to allow a direct interpretation of the uncertainty in the estimation of the states. The FIM is given by sum of the dot product of the output sensitivity for every time step on each grid point:

$$\text{FIM}_{\boldsymbol{S}_y} = \int_0^{t_t} \boldsymbol{S}_y(t)^T\boldsymbol{S}_y(t)dt \tag{28}$$

For the output SA, the diagonal of $\text{FIM}_{\boldsymbol{S}_y}$ is taken for each simulation time t_t. This diagonal contains information of the sensitivity of the sensor output with respect to the initial-state at every grid point. In the analysis, the same cases as in Section 4.1 are studied. Hence, in the first case, in which diffusion dominates the system, as described in Equation (11), four different diffusion rates $a = 0.00002$, $a = 0.0002$, $a = 0.002$, $a = 0.02$ (m^2/s), and $c = 0$ (m/s), $r = 1$ (1/s) and $\alpha = 1$ (°C) are used. For the second case, in which convection dominates the same system, $a = 0.00002$ (m^2/s), and four different convection rates $c = 0.5$, $c = 1.0$, $c = 1.5$, $c = 2.0$ (m/s), and $r = 1$ (1/s) and $\alpha = 1$ (°C) are used. In the first case, a length of $L = 1$ is used, and in the second case $L = 4$ is used. For both cases, the sensor is located at $z = L - 0.1$ (m). The results for the output SA are shown in Figure 4. In the left panel of Figure 4, the diagonal of $\text{FIM}_{\boldsymbol{S}_y}$ for the diffusion-dominant case is shown. The right panel of 4 shows the diagonal of $\text{FIM}_{\boldsymbol{S}_y}$ for the convection-dominant case.

An increase in the diffusion rate, as well as an increase in the convection rate, will give an increase of the output sensitivity over length (L). The increasing output sensitivity over the whole length for increasing diffusion and convection rates results in a decreasing output sensitivity around the point the sensor is located. The sensitivity between the initial-state and the output grows in the first few seconds, but converges to zero for time to infinity. This dynamic behaviour is shown in Figure 5. Notice from Figure 5 that the sensitivity from initial-state-to-output on the interval $z \in [0, 1.5]$ is very small. Hence, to obtain reliable state estimates on this interval, an accurate and sensitive sensor should be used. The sensitivity from the initial state to the output S_y for $z = 0$ (m) and $t = 3$ (s) is equal to 0.1. Since, S_y is much bigger compared to the tolerances of the numerical errors, changes in the initial state can be observed in the output.

4.3 Non-linear 1D CDR sensitivity fields

So far, a constant air velocity, (c) in Equation (11) is assumed. If the air velocity is not constant, a set of non-linear differential equations result. Hence, instead of an LTI system (4), a non-linear state space model is obtained. The calculation of the sensitivity fields, however, can be

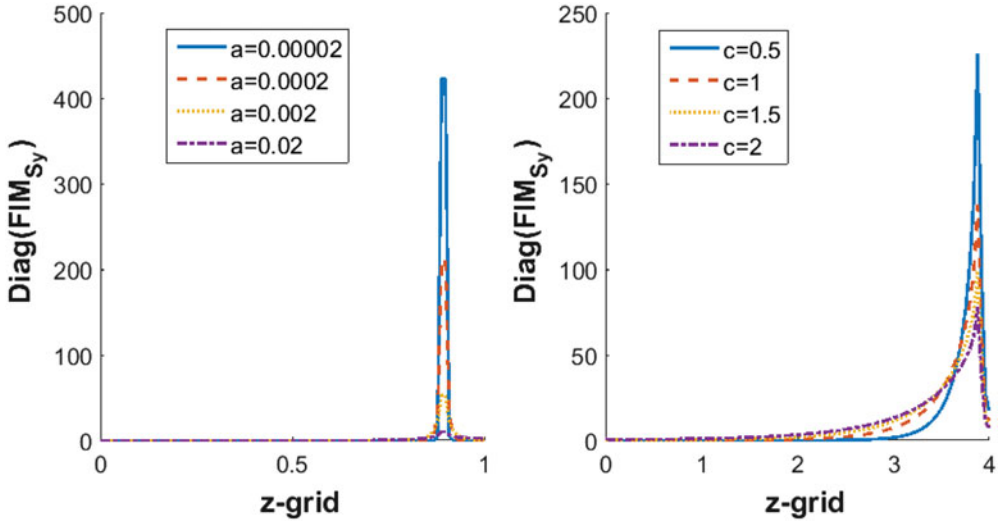

Figure 4. Left, 1D output sensitivity field simulated for different dominant diffusion rates. Right: 1D output sensitivity field simulated for different dominant convection rates. The sensors are placed at $z = L - 0.1$.

directly extended to the non-linear case:

$$\begin{aligned} \dot{\boldsymbol{x}} &= f(\boldsymbol{x}, \boldsymbol{u}), \;\; \boldsymbol{x}(0) = \boldsymbol{x}_0 \\ \boldsymbol{y} &= g(\boldsymbol{x}, \boldsymbol{u}) \end{aligned} \tag{29}$$

The corresponding input ($\boldsymbol{S}_{xu}$) sensitivity equations are given by:

$$\dot{\boldsymbol{S}}_{xu} = \frac{\partial f}{\partial x}\boldsymbol{S}_{xu} + \frac{\partial f}{\partial u} \tag{30}$$

$$\boldsymbol{S}_{yu} = \frac{\partial g}{\partial x}\boldsymbol{S}_{xu} + \frac{\partial g}{\partial u} \tag{31}$$

Here, $\boldsymbol{S}_{xu} :\triangleq \frac{\partial x}{\partial u}$ is the input sensitivity. The sensitivities from the initial states to the output ($\boldsymbol{S}_{yx_0}$) are found from:

$$\dot{\boldsymbol{S}}_{xx_0} = \frac{\partial f}{\partial x}\boldsymbol{S}_{xx_0} + \frac{\partial f}{\partial x_0}, \;\; \boldsymbol{S}_{xx_0}(0) = 1 \tag{32}$$

$$\boldsymbol{S}_{yx_0} = \frac{\partial g}{\partial x}\boldsymbol{S}_{xx_0} + \frac{\partial g}{\partial x_0} \tag{33}$$

Here, $\boldsymbol{S}_{xx_0} := \frac{\partial x}{\partial x_0}$, and $\frac{\partial f}{\partial x_0} = \frac{\partial g}{\partial x_0} = 0$. Furthermore, in both cases, we define the matrices $\boldsymbol{A} := \frac{\partial f}{\partial x}$, and $\boldsymbol{C} := \frac{\partial g}{\partial x}$, whilst in (30) and (31) we define $\boldsymbol{B} := \frac{\partial f}{\partial u}$, and $\boldsymbol{D} := \frac{\partial g}{\partial u}$

5. Input and output sensitivities of 2D coupled thermal flow in bulk storage facilities

Coupled CDR equations typically describe the dynamics of post-harvest storage processes. However, these equations are also used in a wide range of other processes that utilise the laws of conservation of heat and mass (see, for instance, Hsieh & Yang, 2010; Vali, Simonson, Besant, & Mahmood, 2009; Zambra, Munoz, & Moraga, 2015). In

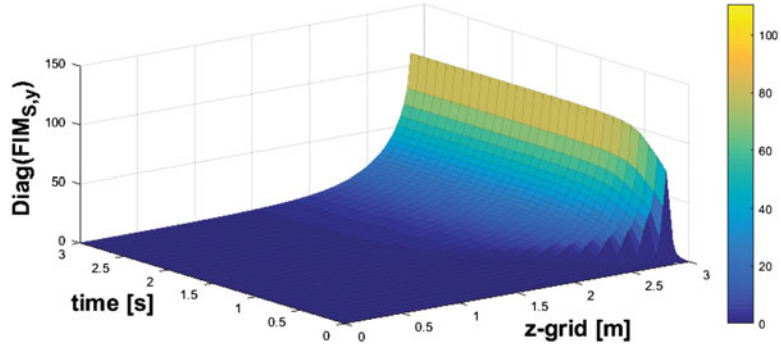

Figure 5. Development in time of 1D output sensitivity field simulated for bulk storage facility, with $a = 0.00002$ (m^2/s), $c = 0$ (m/s), $r = 1$ (1/s), $\alpha = 1$ (°C), $L = 3$ (m) and $\Delta z = L/100$.

Table 1. Paremeter values of the system as in (34).

Parameter	Value	Unit
a_{ax}, a_{ay}	0.00002	(m^2/s)
c_x	1	(m/s)
c_y	0.05	(m/s)
a_{px}, a_{py}	0.0000001	(m^2/s)
r_a	1	(1/s)
r_p	0.0002	(1/s)

the porous medium of a bulk food-storage facility, interaction between the product and the air induces the coupling between the CDR equations that describe temperature in the air and in the food product. For a more detailed analysis of the influence of the actuator and sensors on the states, a 2D simulation will be performed. As before, temperature balances will be used, and these are defined in the spatial coordinates x and y on a $[0, L]$x$[0, L]$ domain:

$$\begin{aligned}
\frac{\partial T_a}{\partial t} &= a_{ax}\frac{\partial^2 T_a}{\partial x^2} + a_{ay}\frac{\partial^2 T_a}{\partial y^2} \\
&\quad -c_x\frac{\partial T_a}{\partial x} - c_y\frac{\partial T_a}{\partial y} - r_a T_a + r_a T_p \\
T_a(x,0,t) &= \alpha, \quad \text{for } x \in \left[0, \frac{L}{2}\right], \\
T_a(x,0,t) &= 0, \quad \text{for } x \in \left[\frac{L}{2}, L\right], \\
\frac{\partial T_a}{\partial x}(x,L,t) &= 0, \\
\frac{\partial T_a}{\partial y}(0,y,t) &= 0, \quad \frac{\partial T_a}{\partial y}(L,y,t) = 0 \\
\frac{\partial T_p}{\partial t} &= a_{px}\frac{\partial^2 T_p}{\partial x^2} + a_{py}\frac{\partial^2 T_p}{\partial y^2} - r_p T_p + r_p T_a \\
\frac{\partial T_p}{\partial x}(0,y,t) &= 0, \quad \frac{\partial T_p}{\partial x}(L,y,t) = 0, \\
\frac{\partial T_p}{\partial y}(x,0,t) &= 0, \quad \frac{\partial T_p}{\partial y}(x,L,t) = 0
\end{aligned} \tag{34}$$

Here, T_a is the air temperature, T_p the product temperature, a_{ax}, a_{ay} the diffusion coefficient of air in x direction and y direction respectively, c_x, c_y the convection coefficient of air in x direction and y direction respectively, a_{px}, a_{px} the diffusion coefficient of the product in x direction and y direction respectively, and r_a and r_p a reaction coefficient expressed as a heat transfer coefficient.

For the simulations of the system (34), the parameters, as in Table 1, are used. Notice that the system has relative fast (air-) and slow (product-) properties, which will have influence on the simulations.

For the evaluation of the input sensitivity of the 2D system, the actuator is, as in the 1D case, located at the bottom of the configuration at $y = 0$ (see Figure 6). Notice that the actuator acts only on the left half. The actuator operates at a constant velocity and input temperature. The actuator only acts on the air domain, and by the interaction between the air and the product the temperature in the product domain is affected. Hence, a Dirichlet boundary condition is prescribed at $y = 0$. At all other boundaries, a Neumann boundary condition is prescribed (Figure 6). A grid of 30×30 is used for the calculations. Due to the coupling between air and product, a system matrix of 1800×1800 ($30{\cdot}30{\cdot}2 = 1800$ states) is produced. In the simulation only, the air temperature at $y = 0$ can be influenced. As the sensitivities are time-dependent, different simulation times could be taken to investigate the influence of the input on the states. The steady state value of the sensitivity field is reached as time (t) goes to infinity. A large simulation time gives a good approximation of steady state value, hence a simulation time of $t = 400$, with steps of 0.001 (s) is taken.

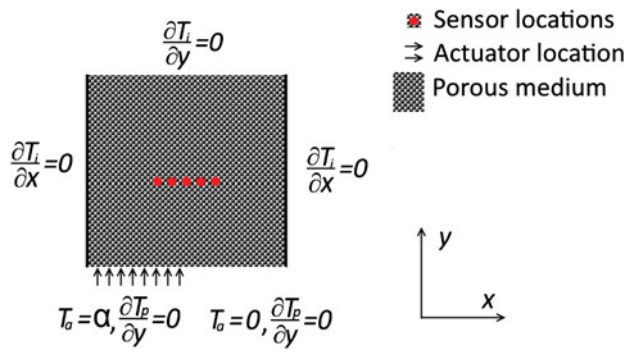

Figure 6. 2D configuration of the porous medium. Located at the bottom the inlet of the bulk system is one actuator on the left-hand side. The sensors are placed in the centre of the bulk.

The result of the steady state SA of the actuator on the states is shown in Figure 7. As expected, the state is most sensitive at the bottom, where the actuator is located. The sensitivities show a homogeneous profile in the x-direction for $x \in [0, \frac{L}{2}]$. Despite the velocity component d in horizontal direction, the sensitivity of the state for $x \in [\frac{L}{2}, L]$ is very small. In the y-direction, an exponential decrease is obtained. Likewise as in the 1D case, the total sensitivity of the input on the states is increased for longer time periods.

For the analysis of the output, sensitivity fields initially the sensors are place in the air domain at $y = 1.8$ and for $x \in [\frac{L}{3}, \frac{2L}{3}]$, see Figure 6. As follows, a simulation of time of 15 seconds with steps of 0.001 (s) and a grid of 12×12 are used. The results are shown in Figure 8. Notice that at the bottom ($y = 0$), the sensitivity is very small, but larger than one. Around the sensor location, the highest sensitivities are obtained. Despite the low horizontal velocity,

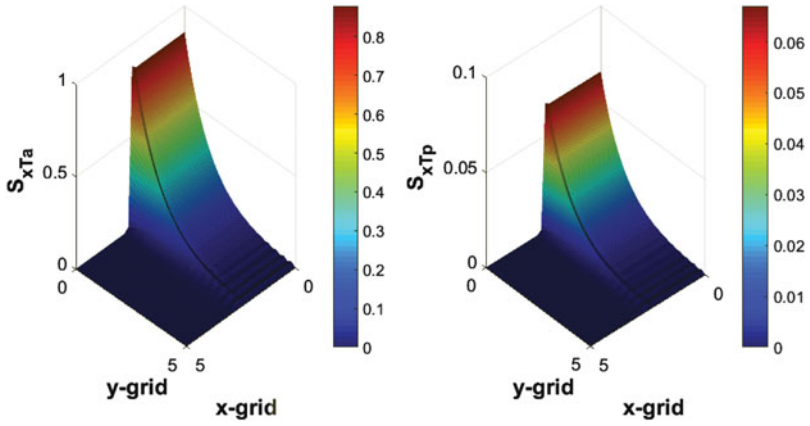

Figure 7. Input sensitivity field of the coupled 2D CDR-system, $t = 400$ (s) and 30x30 grid. Left, 2D input sensitivity field related to T_a. Right, 2D input sensitivity field related to T_p.

also in horizontal direction a relatively high sensitivity is obtained.

Figures 7 and 8 show results where in some areas and on a specific time instant the input or output sensitivity is close to zero and thus indicating locally uncontrollable or unobservable states. The results also indicate that for larger simulation time the input sensitivity and diagonal element of the FIM will increase. However, in practice, the dominant response time of the system (τ) leads. For the air domain, we would typically act or sample ever 0.1–0.2τ. Thus, if, for instance, the input or output sensitivity are close to zero on a time range $[0\ ,\ 0.2\tau]$, the controlled or observed system can be practically considered as uncontrollable or unobservable.

The results of this section can lead to more efficient ventilation strategies in bulk storage facilities, as the actuator and sensor locations can be re-designed by the sensitivity results. For example, the actuator location can be chosen such that the input has a stronger influence on the states in the whole domain. In the y-direction with the actuator located at $([0, \frac{L}{2}],0)$, small sensitivities are obtained in the top layer. To gain more influence on the states in the top layer the geometry of the storage facility, or the actuator functionality should be re-designed. In practice a better performance could be obtained, for instance, if the fan depicted in Figure 1 switches after a certain time period from blowing to suction.

From the results of the output sensitivity field, the observable region inside the bulk is known. From Figure 8, it can be seen that in case of an air temperature sensor also a relatively large sensitivity for the product temperature is obtained. Thus, for climate controlled bulk facilities, the results give supporting information on the number, the best location and the choice of the sensors. Also, for the implementation of model-based quality control in bulk storage facilities, input and output sensitivity fields are of great interest for the choice of actuators and sensors and their location.

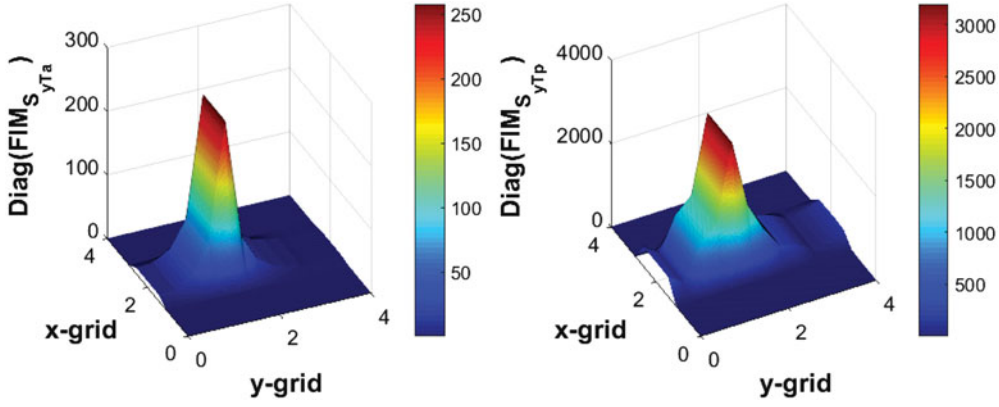

Figure 8. Output sensitivity field of the coupled 2D CDR-system. Left, 2D output sensitivity field related to T_a. Right, 2D output sensitivity field related to T_p.

On nD domains, with $n \geq 3$, SVD of the sensitivity matrices may be helpful to support the interpretation of the sensitivity fields. For more complex problems in higher dimensions, we also foresee numerical issues that need to be tackled. For further understanding and application of the theory presented in the article, further research on sensitivity fields for special classes of infinite-dimensional systems is needed.

6. Conclusion

In this paper, we analysed the controllability and observability properties of spatially distributed thermal flow in bulk storage facilities. The classical system theory concepts, controllability and observability, not only provide limited, but crucial, information, but also unreliable results, due to matrix multiplications of the discretised system with fine mesh. The information from a controllable or observable analysis is insufficient because in practice, we are only interested to find out if it is possible to have some influence on a certain state, or if a certain state can be observed during a certain time period. The SVD gives additional information on which states are controllable/uncontrollable or observable/unobservable. However, due to the matrix computations, small discretisation steps result in numerical errors in the singular values.

By introducing input and output sensitivity fields, whilst using the discretised state space representation, the aforementioned problems are avoided. The sensitivity field of the input to state gives information about the influence, and thus practical controllability, of the input on a state for a specific time period. Changing the time period results in other controllable/uncontrollable states. The sensitivity field of the output to state gives information about the practical observability of the each state over a specific time period. Likewise, as for controllability, a increase or decrease of the time period results in other observable/unobservable states. In conclusion, sensitivity fields, provide, from a practical perspective, valuable information about the influence of the input-to-state and the initial-state on the output, respectively.

Acknowledgments

This work is part of a research project carried out at and financially supported by Omnivent Techniek B.V., in the Netherland: an international specialist in food-storage including the storage of potatoes, onions, carrots and other fruits and vegetables. This research project will provide Omnivent Techniek B.V. with more information and knowledge about how storage- and control strategies influence potato-quality and storage losses.

Disclosure statement

No potential conflict of interest was reported by the authors.

Funding

Omnivent Techniek B.V. grant number [21032014].

References

Amouroux, M., Jai, A.E., & Zerrik, E. (1994). Regional observability of distributed systems. *International Journal of Systems Science*, *25*, 301–313.

Brecht, A.V., Quanten, S., Zerihundesta, T., Buggenhout, S.V., & Berckmans, D. (2005). Control of the 3-D spatio-temporal distribution of air temperature. *International Journal of Control*, *78*, 88–99.

Cheney, W., & Kincaid, D. (2008). *Numerical mathematics and computing*. Belmont, USA: Thomson Brooks/Cole.

Chourasia, M., & Goswami, T. (2007). Three dimensional modeling on airflow, heat and mass transfer in partially impermeable enclosure containing agricultural produce during natural convective cooling. *Energy Conversion and Management*, *48*, 2136–2149.

Curtain, R.F., & Zwart, H. (1995). *An introduction to infinite dimensional linear systems theory*. New York, NY: Springer.

Dickinson, R.P., & Gelinas, R.J. (1976). Sensitivity analysis of ordinary differential equation systems; A direct method. *Journal of computational physics*, *21*, 123–143.

Dochain, D., Couenne, F., & Jallut, C. (2009). Enthalpy based modelling and design of asymptotic observers for chemical reactors. *International Journal of Control*, *82*, 1389–1403.

Doren, J.F.M.v., Hof, P.M.J.v.d., Bosgra, O.H., & Jansen, J. (2013). Controllability and observability in two-phase porous media flow. *Computational Geosciences*, *17*, 773–788.

Friedland, B. (2005). *Control System Design: An introduction to state-space methods*. Mineola, NY: Dover Publicatoins.

Garzon-Alvarado, D.A., Galeano, C.H., & Mantilla, J.M. (2012). Computational examples of reaction-convection-diffusion equations solution under the influence of fluid flow: First example. *Applied Mathematical modelling*, *36*, 5029–5045.

Grubben, N.L.M., & Keesman, K.J. (2015). Modelling ventilated bulk storage of agromaterials: A review. *Computers and Electronics in Agriculture*, *114*, 285–295.

Hsieh, P.W., & Yang, S.Y. (2010). Two new upwind difference schemes for a coupled system of convection diffusion equations arising from the steady MHD duct flow problems. *Journal of Computational Physics*, *229*, 9216–9234.

Jai, A.E., Simon, M.C., Zerrik, E., & Pritchard, A.J. (1995). Regional controllability of distributed parameter systems. *International Journal of Control*, *62*, 1351–1365.

Kalman, R. (1959). On the general theory of control systems. *IRE Transactions on Automatic Control*, *4*(3), 110–110.

Kwakernaak, H., & Sivan, R. (1972). *Linear optimal control systems*. New York, NY: Wiley.

Lopes, R.J.G., & Quita-Ferreira, R.M. (2011). Numerical assessment of diffusion-convection-reaction model for the catalytic abatement of phenolic wastewaters in packed-bed

reactors under trickling flow conditions. *Computers and Chemical Engineering*, *35*, 2706–2715.

Lukasse, L.J.S., de Kramer-Cuppen, J.E., & Voort, A.J.v.d. (2007). A physical model to predict climate dynamics in ventilated bulk-storage of agricultural produce. *International Journal of Refrigeration*, *30*, 195–204.

Lynch, D.R. (2005). *Numerical partial differential equations for environmetal scientists and engineers*. Dartmouth, New Hampshire: Springer.

Mohammadi, L., Aksikas, I., Dubljevic, S., & Forbes, J. (2012). LQ-boundary control of a diffusion-convection-reaction system. *International Journal of Control*, *85*, 171–181.

Moler, C. (2004). *Numerical computing with MATLAB*. Philadelphia: Society for industrial and applied mathematics.

Nagarajan, V., Chen, Y., Wang, Q., & Ma, T. (2015). CFD modeling and simulation of sulfur trioxide decomposition in ceramic plate-fin high temperature heat exchanger and decomposer. *International Journal of Heat and Mass Transfer*, *80*, 329–343.

Saltelli, A., Chan, K., & Scott, E.M. (eds.). (2000). *Sensitivity analysis*. New York, NY: Wiley.

Storkaas, E., & Skogestad, S. (2007). Controllability analysis of two-phase pipeline-riser systems at riser slugging conditions. *Control Engineering Practice*, *15*, 567–581.

Tomovic, R. (1963). *Sensitivity analysis of dynamic systems*. New York, NY: McGraw-Hill.

Vali, A., Simonson, C.J., Besant, R.W., & Mahmood, G. (2009). Numerical model and effectiveness correlations for a run-around heat recovery system with combined counter and cross flow exchangers. *International Journal of Heat and Mass Transfer*, *52*, 5827–5840.

Varga, E., Hangos, K., & Szigeti, F. (1995). Controllability and observability of heat exchanger networks in the time-varying parameter case. *Control Engineering Practice*, *3*(10), 1409–1419.

Zambra, C.E., Munoz, J.E.F., & Moraga, N.O. (2015). A 3D coupled model of turbulent forced convection and diffusion for heat and mass transfer in a bioleaching process. *International Journal of Heat and Mass Transfer*, *85*, 390–400.

Zandvliet, M., Doren, J.F.M.v., Bosgra, O.H., Jansen, J., & Hof, P.M.J.v.d. (2008). Controllability, observability and identifiability in single-phase porous media flow. *Computational Geosciences*, *12*(4), 605–622.